Kinematic Fit Studies of the Channel $K^+ \to \pi^+\pi^0$

I. O. Skillicorn,* D. Protopopescu,† and D. Britton
University of Glasgow, Glasgow G12 8QQ, UK
(Updated: September 18, 2018)

Selected reconstructed NA62 data and Monte Carlo events for the channel $K^+ \to \pi^+\pi^0$ have been studied using kinematic fitting. The improvement of the resolution in missing mass and and gamma-gamma mass as a result of the constrained fit is demonstrated. The χ^2 and pulls of the fits have been examined to check the event selection and accuracy of the reconstruction.

I. INTRODUCTION

Energy-momentum constrained least squares fits have been made to the beam (K^+) and spectrometer (π^+) tracks plus two gammas measured in the Liquid Krypton detector (LKr).

The fits were made using the package APLCON for 12 parameters subject to 4 constraints [1]. The standard $K^+ \to \pi^+\pi^0$ selection code [2], run on 2016 data and on Monte Carlo (MC), was used to provide input for the fits. The fit parameters were momentum $\mathbf{p}$, dx/dz and dy/dz for the four measured particles.

Initially, the covariance matrix was taken to be diagonal with error estimates from [3, 4]. Subsequently, for both data and MC, the errors have been adjusted to get the RMS of the pulls within 10% of unity (for details see Appendix A and Ref. [5]).

The object of this study was to examine the χ^2 and pulls of the fit to both data and MC to check consistency with the $K^+ \to \pi^+\pi^0$ hypothesis, check the error estimates, identify systematic errors, and determine the influence of the fit on the measurement accuracy of the tracks and the missing mass.

This work complements that of M. Corvino [7].

II. RESULTS

The results of the kinematic fits to data and Monte Carloare shown in Figures 1 to 12.

Figure 1 compares the probability distributions and χ^2 for data and Monte Carlo. The probability distribution would be flat for a correctly measured set of events consistent with the assumed hypothesis $K^+ \to \pi^+\pi^0$. The plots suggest that $\sim$ 95 % of events are well measured while the remainder are either badly measured or are otherwise incompatible with the $K^+ \to \pi^+\pi^0$ hypothesis.

Figures 2 and 3 show the influence of the fit on the missing mass to the $K^+\pi^+$ system, and the gamma-gamma mass, respectively:

$$\begin{aligned} m_m^2 &= (P_{K^+} - P_{\pi^+})^2 \\ m_{\gamma\gamma}^2 &= (P_{\gamma 1} + P_{\gamma 2})^2 \end{aligned}$$

where P_i are four-vectors.

Data and MC are similar. The fit reduces the width of the missing mass distribution by about a factor of four and the gamma-mass width by about a factor of two.

Figure 4 plots the closest distance of approach (CDA) before and after the kinematic fitting. The fit has little effect on the CDA. The CDA is somewhat broader for the MC than the data.

Figures 5 to 8 show the effect of the fit on the errors in the fitted parameters. The influence of the fit is strongly parameter dependent but similar for data and MC.

The pulls for the data and MC are plotted in Figures 9 to 12. Pulls are defined as

$$P = \frac{x_{meas} - x_{fit}}{\sqrt{\sigma_{meas}^2 - \sigma_{fit}^2}}$$

The mean values of the pulls are given in the Figures 9 to 12 and listed in Table I.

In the absence of systematic effects due to measurement or reconstruction the pulls would have a mean value of zero. In Table I the entries in bold differ significantly from zero. For the data, the systematic effects are evident for dx/dz, while for the MC they are present for dy/dz. For both data and Monte Carlo, the shift in the K^+ parameters is in the opposite direction to that for the gammas detected in the LKr, as might be expected from energy-momentum conservation.

*Electronic address: Ian.Skillicorn@glasgow.ac.uk
†Electronic address: protopop@cern.ch

Fit parameter		Mean pull	
		Data	MC
π^+	P	-0.175	0.025
	dx/dz	-0.204	-0.045
	dy/dz	0.099	0.089
K^+	P	0.200	-0.054
	dx/dz	**0.543**	-0.147
	dy/dz	-0.135	**-0.395**
γ_1	P	0.001	-0.128
	dx/dz	**-0.586**	0.216
	dy/dz	0.152	**0.470**
γ_2	P	-0.050	0.039
	dx/dz	**-0.526**	0.203
	dy/dz	0.152	**0.405**

TABLE I: Mean pull values. Note that the entries in **bold** differ significantly from zero.

III. SUMMARY

Events from the channel $K^+ \to \pi^+\pi^0$ have been selected from NA62 2016 data and MC using the `KaonEventAnalysis.cc` analysis code. The selected events have been fitted to $K^+ \to \pi^+\pi^0$ using the least squares fitting program APLCON. The four-constraint fit was made to the twelve parameters (momentum and two track slopes for each particle) describing the K^+, π^+ and the two γ from the π^0 decay. In this analysis the **input** measurement error matrix has been taken to be diagonal, i.e. we have assumed that there are no correlations between the input variables (the fitted output variables are, of course, strongly correlated).

After error correction, ∼95% of data and MC events give a four-constraint fit with the flat probability distribution expected for events consistent with the channel $K^+ \to \pi^+\pi^0$.

The fit probability distribution has a peak at low probability that implies that ∼5% of the selected events are incompatible with the assumed $K^+ \to \pi^+\pi^0$ hypothesis. For the MC events, the pulls suggest that these low probability events result from mis-measurement of the gammas in the LKr.

The pulls for the tracks give indications of systematic errors in reconstruction of about half a standard deviation. These are in the beam and gamma dx/dz slopes for data, and the beam and gamma dy/dx slopes for MC.

IV. APPENDIX A

Figures 13 to 15 show the fit probability distribution and pulls for the 4-constraint fits using errors from [3, 4] i.e. prior to correcting the input measurement errors to obtain the results shown in Figures 1 to 12.

Figure 13 shows a non-uniform probability distribution with a peak at low probabilities that demonstrates that the input errors are, in general, underestimated. The degree of undestimation is shown by the RMS of the pulls; for example, the pull for the track momentum suggests that the errors for this variable should be increased by a factor 1.515 (see Figure 14). In practice, due to correlations between the fitted variables, it was found neccesary to iterate the error correction to get unit-width pulls.

V. APPENDIX B

To illustrate the usefulness of a one-constraint fit we show in this Appendix the p-distributions for several time measurements: for these variables a departure from a flat p-distribution corresponds to a non-Gaussian time distribution.

Here, `Kmu2` events have been selected and the time distributions $t_{GKT} - t_{KTAG}$, $t_{STRAW} - t_{KTAG}$, $t_{RICH} - t_{KTAG}$ and $t_{CHOD} - t_{KTAG}$ have been plotted as p-values from a χ^2 for 1 degree of freedom.

Figures 16 and 17 show the distributions for these p-values. With the exception of the $t_{CHOD} - t_{KTAG}$ (Fig.17b), the distributions are approximately flat, which is consistent with Gaussian time distributions. This suggests a problem with the CHOD timing. More details can be found in [6].

This time information could be added into the χ^2 and/or the constraints in the kinematic fit to enhance the hypothesis identification.

[1] V. Blobel, Constrained Least Squares, see documentation at http://www.desy.de/∼blobel/wwwcondl.html. A C++ wrapper written by A.Neiser is available at https://github.com/neiser/APLCON .

[2] G. Ruggiero, `KaonEventAnalysis` analysis code, part of the NA62FW software package, (retrieved May 2018), see https://gitlab.cern.ch/NA62FW

[3] P. d'Argent *et al.*, arXiv:1703.08505, JHEP **1705** (2017) 143

[4] V. Fanti *et al.*, NIM A 574 (2007) 433

[5] I. O. Skillicorn, details online at http://www.ppe.gla.ac.uk/∼skilli/na62pifit4.html

[6] I. O. Skillicorn, details online at http://www.ppe.gla.ac.uk/∼skilli/na62mutime.html

[7] M. Corvino, KinFit description online at http://indico.cern.ch/event/664737/contributions/2715027

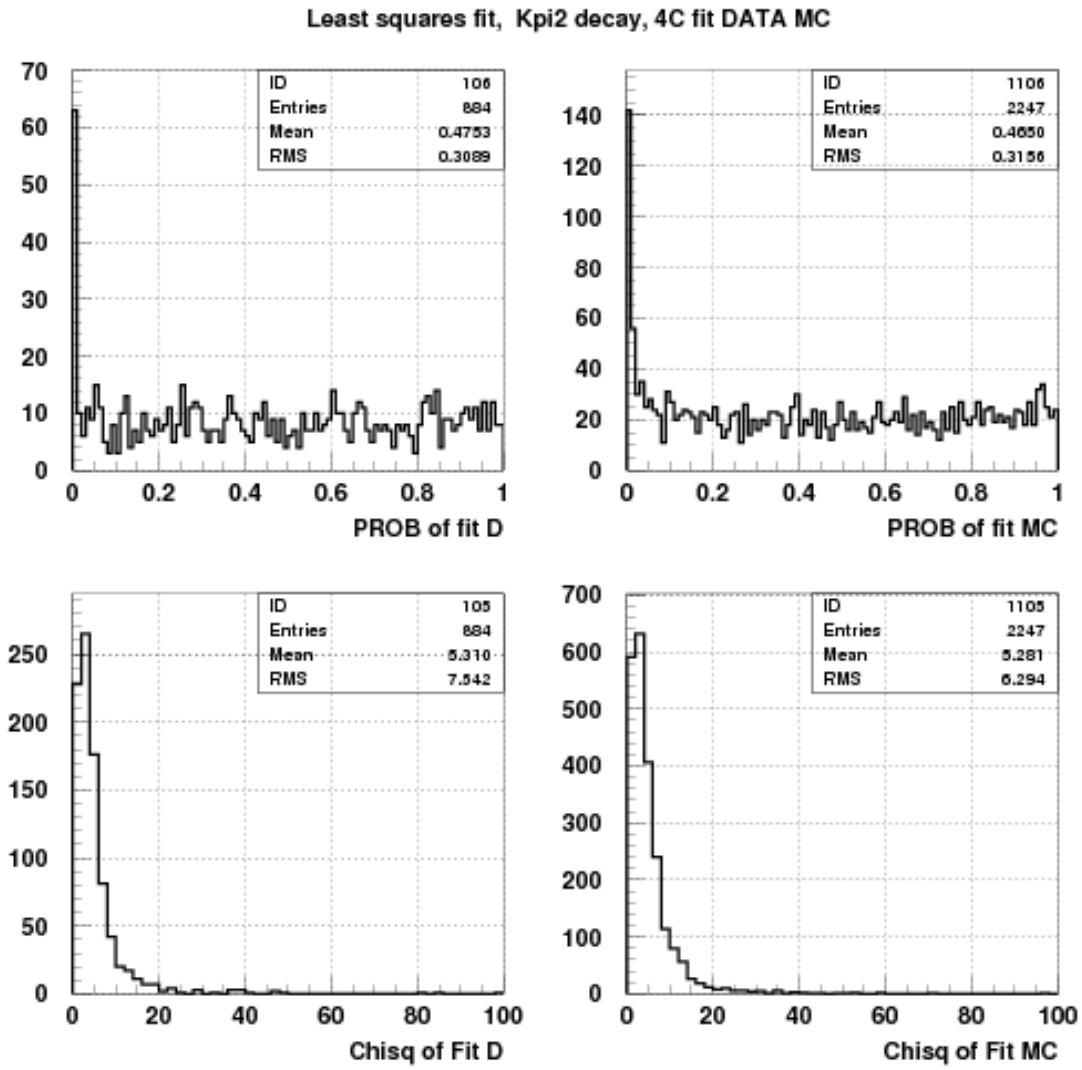

FIG. 1: Probability and χ^2 distributions for data (left column) and MC (right column).

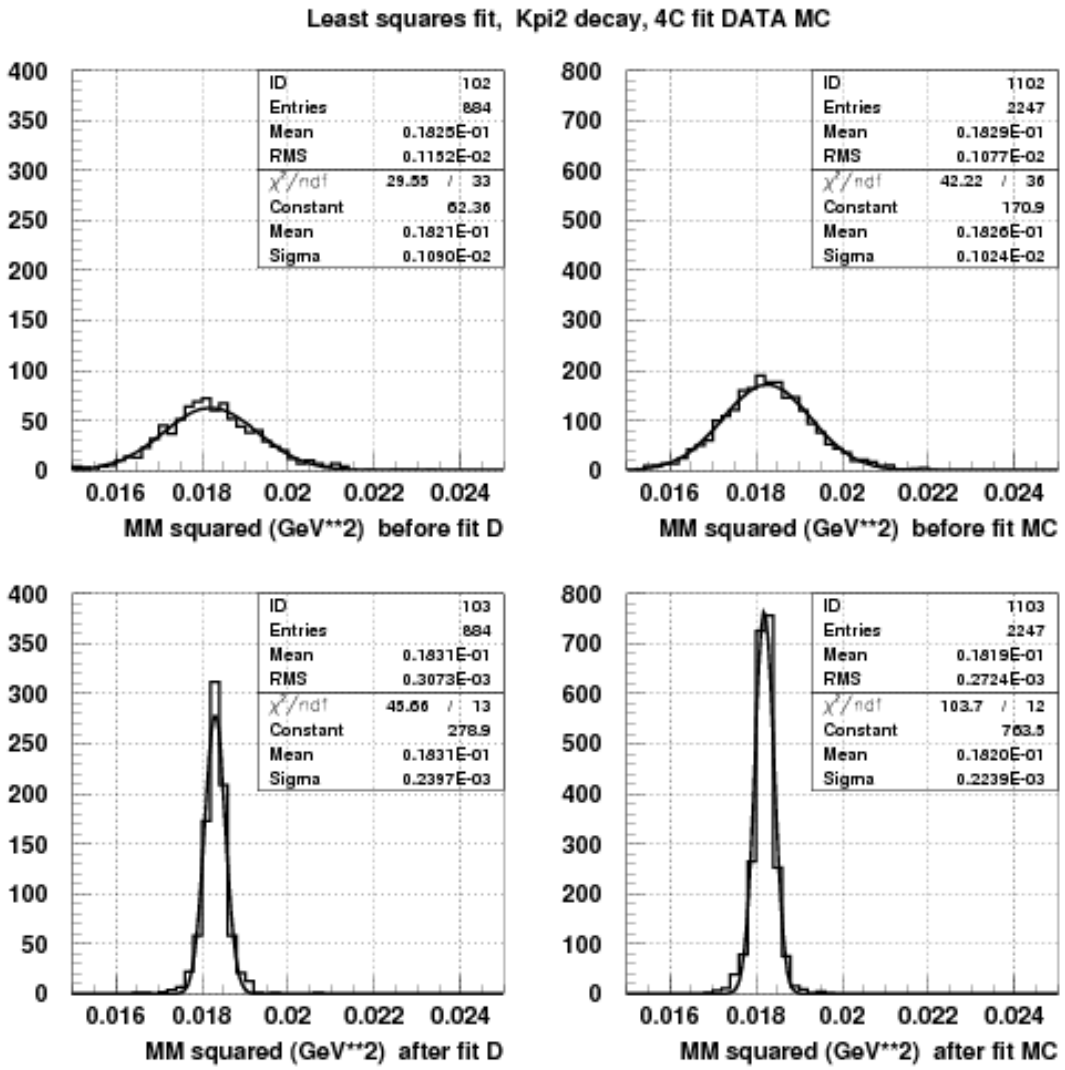

FIG. 2: Missing mass squared distributions before (top row) and after (bottom row) kinematic fitting for data (left column) and Monte Carlo (right column).

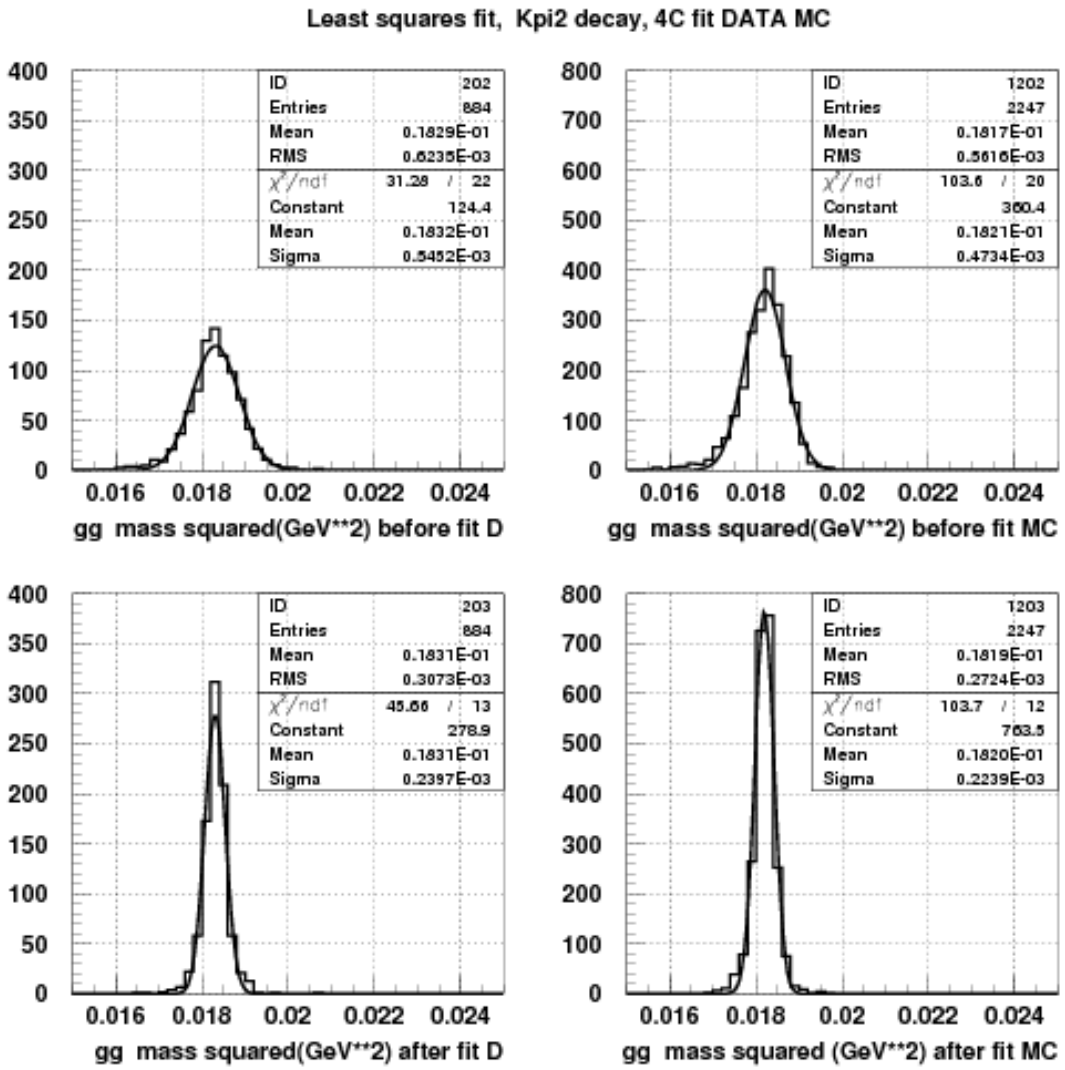

FIG. 3: Gamma-gamma mass squared distributions before (top row) and after (bottom row) kinematic fitting for data (left column) and Monte Carlo (right column).

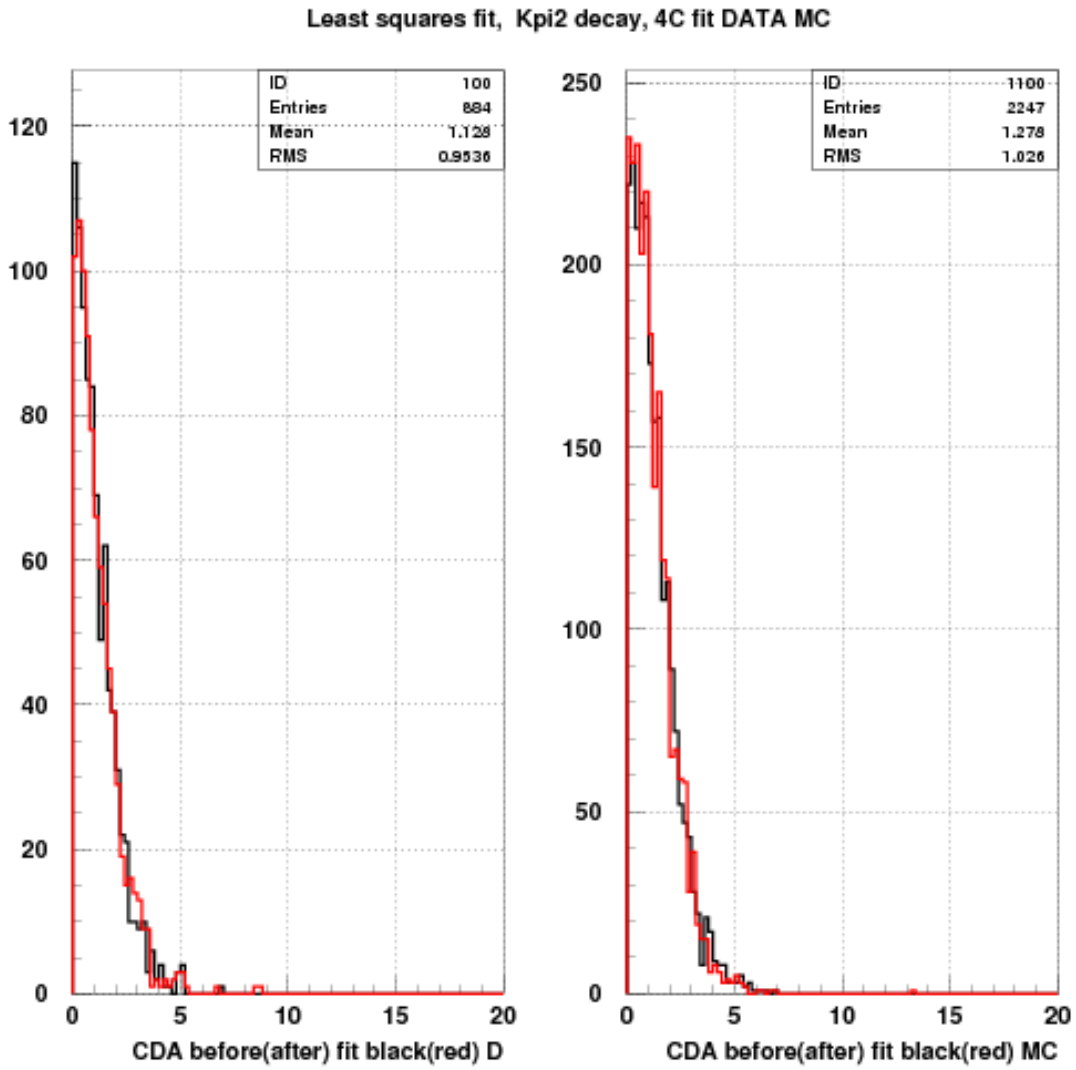

FIG. 4: CDA distributions before (black line) and after fit (red line) for data (left column) and Monte Carlo (right column).

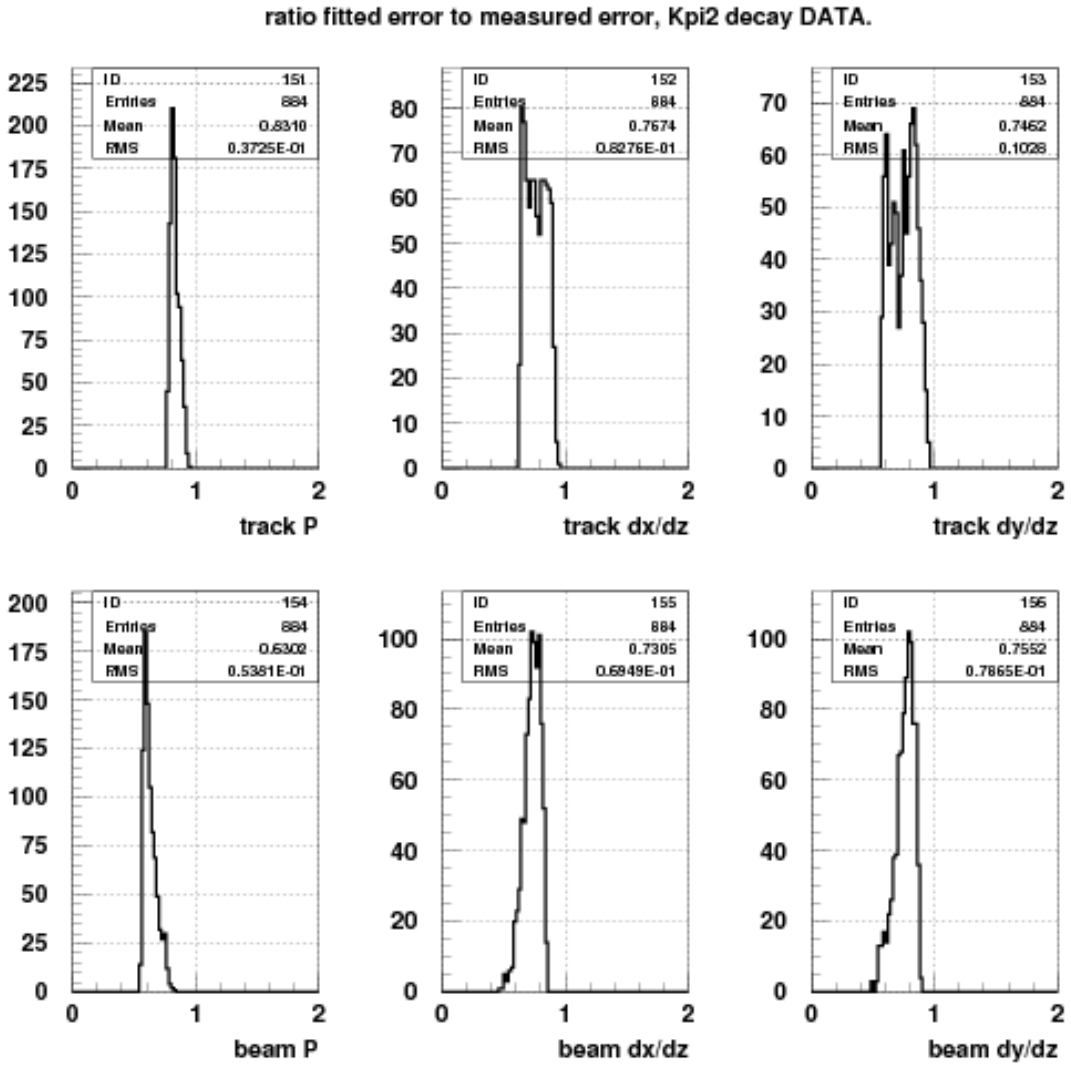

FIG. 5: Data: Ratio of fitted error to measured error for the track (top row) and beam (bottom row) variables.

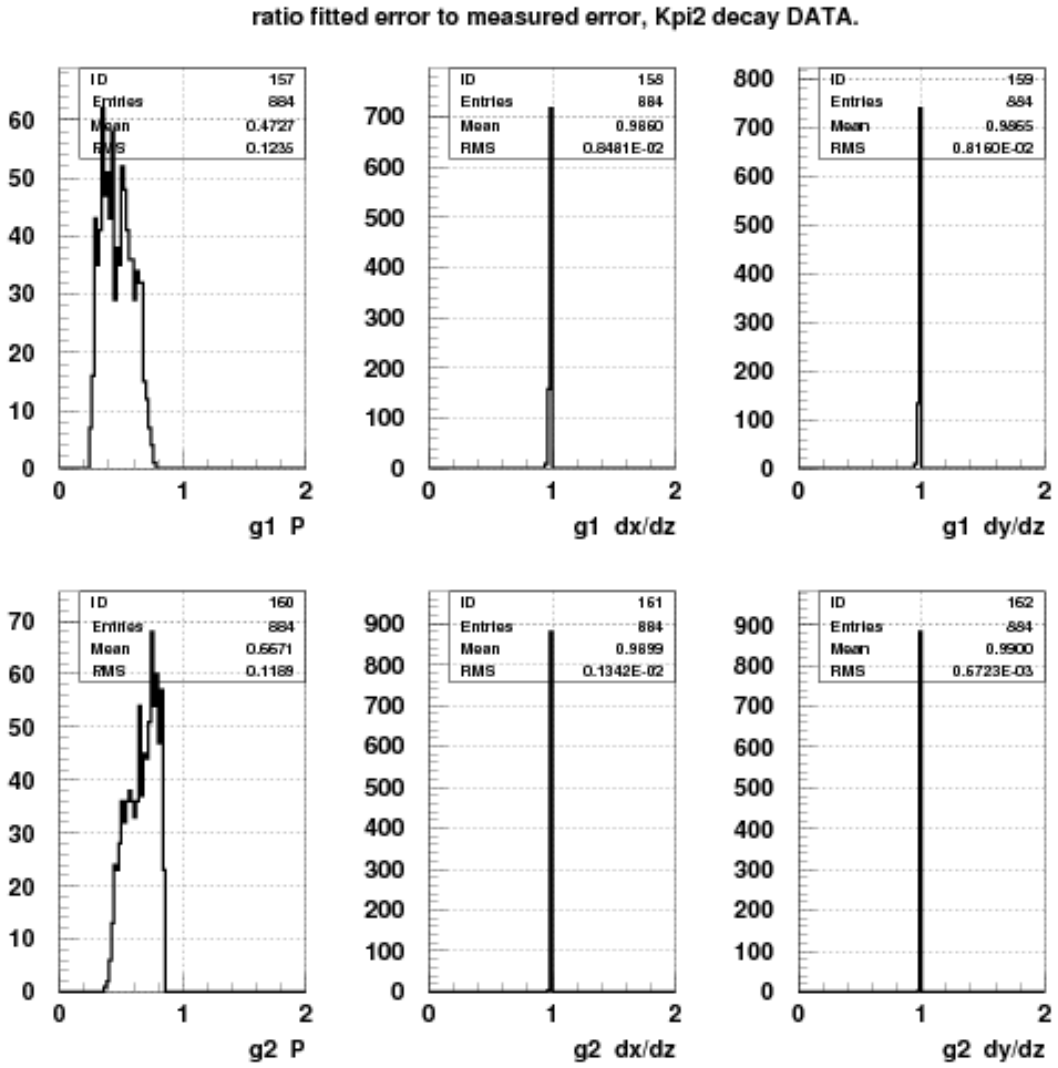

FIG. 6: Data: Ratio of fitted error to measured error for the two gammas (one per row).

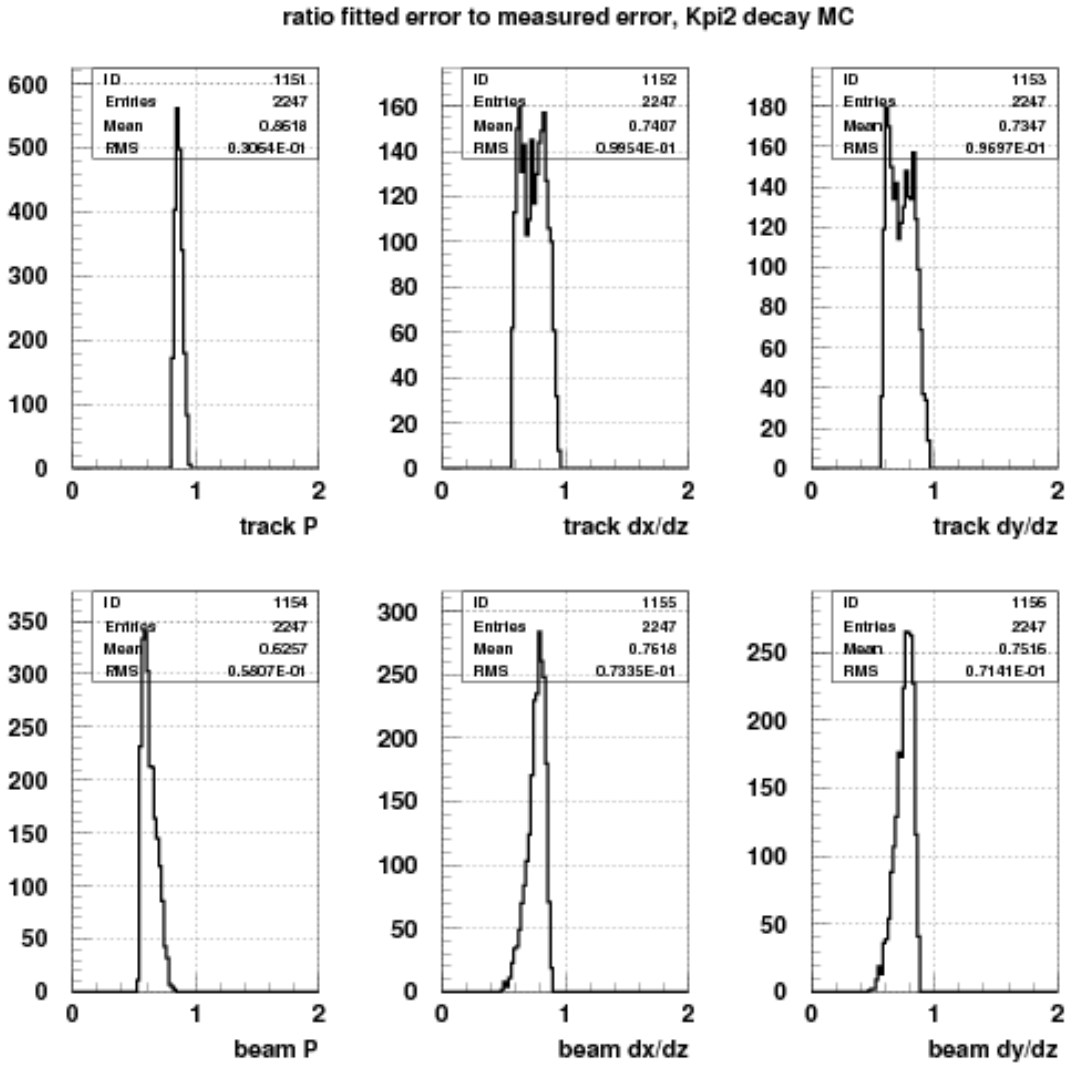

FIG. 7: Monte Carlo: Ratio of the fitted error to the measured error for the track (top row) and beam (bottom row).

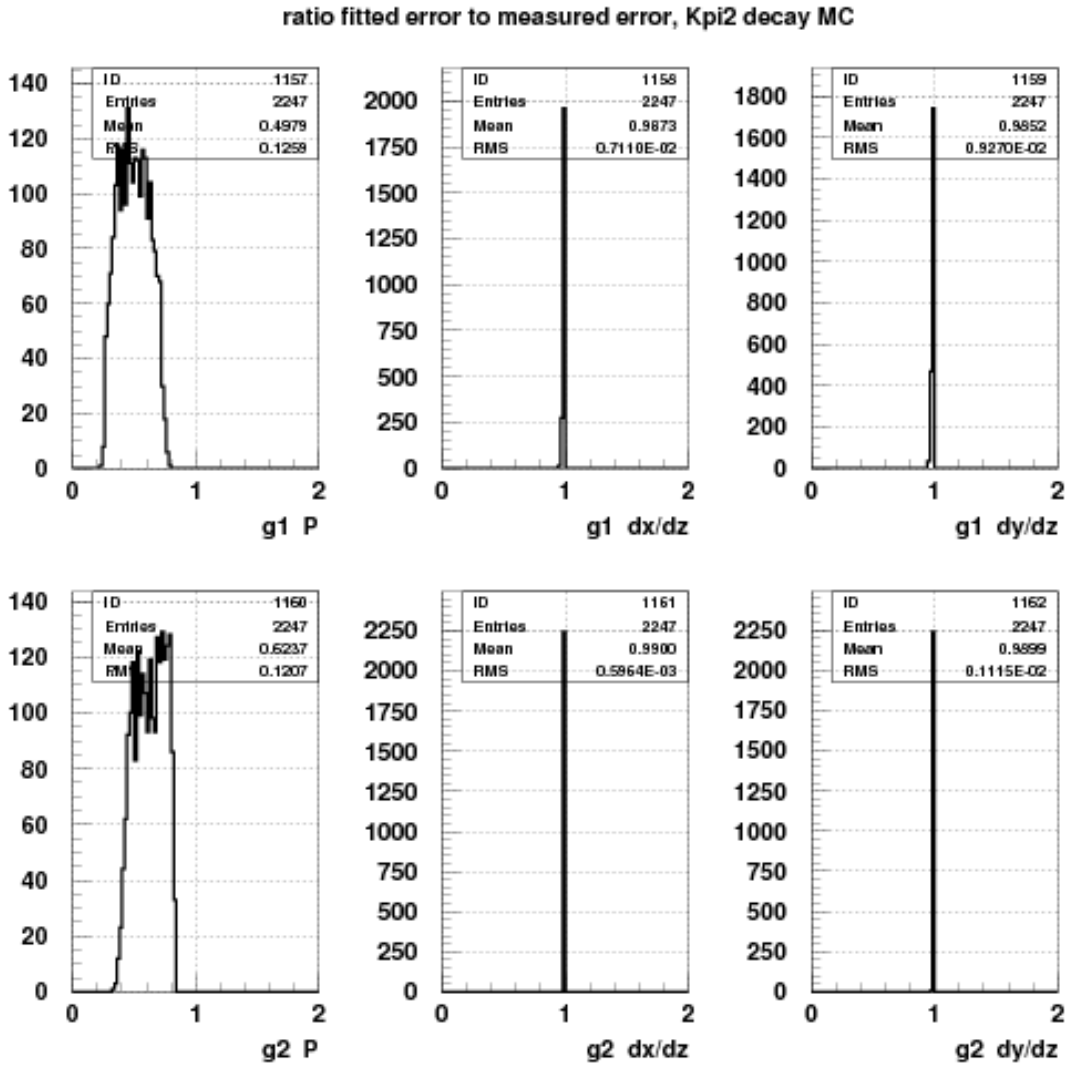

FIG. 8: Monte Carlo: Ratio of the fitted error to the measured error for the two gammas (one per row).

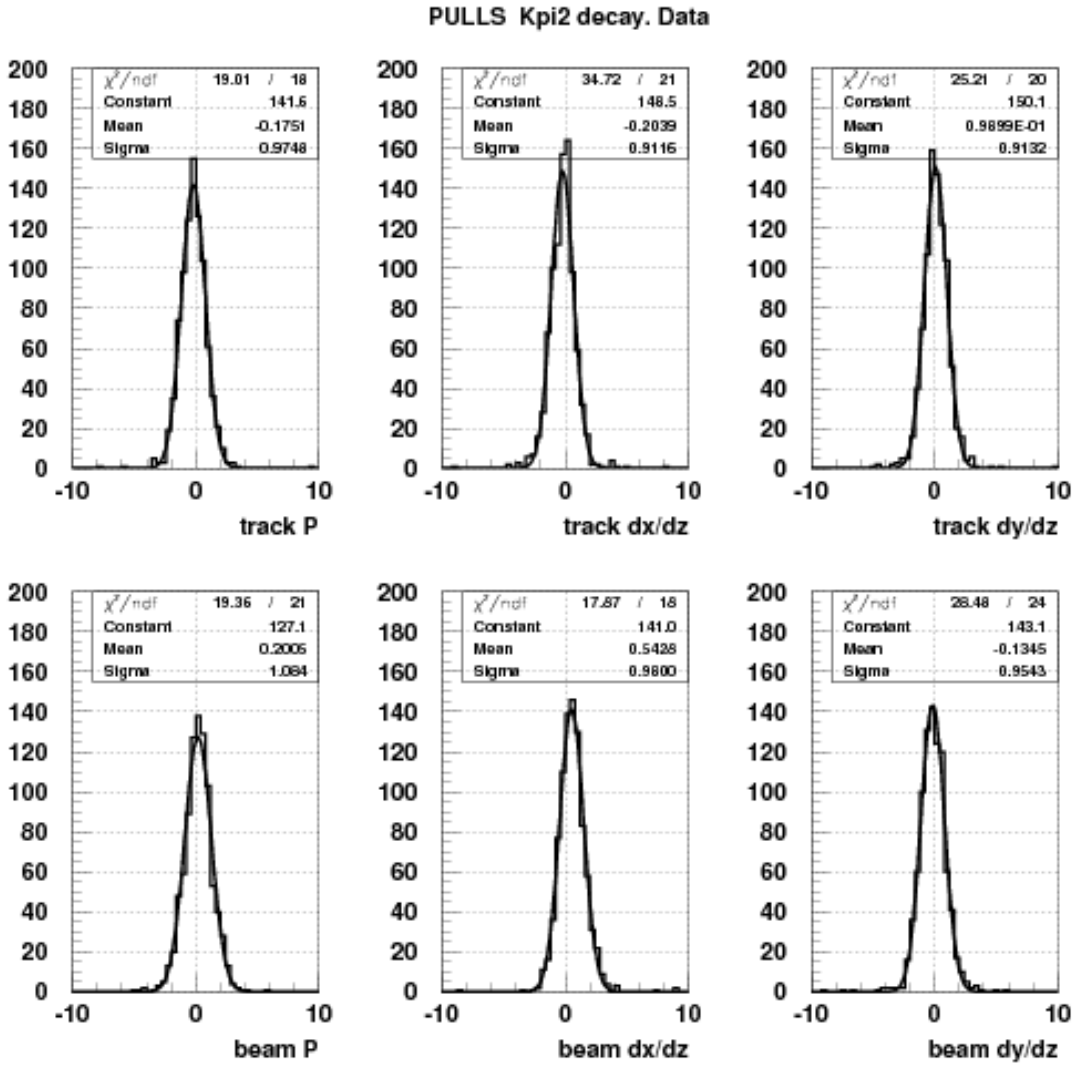

FIG. 9: Data: Pulls for momenta $\mathbf{p}$ (first column) and slopes (dx/dz, dy/dz), for the pion track (top row) and beam (bottom row).

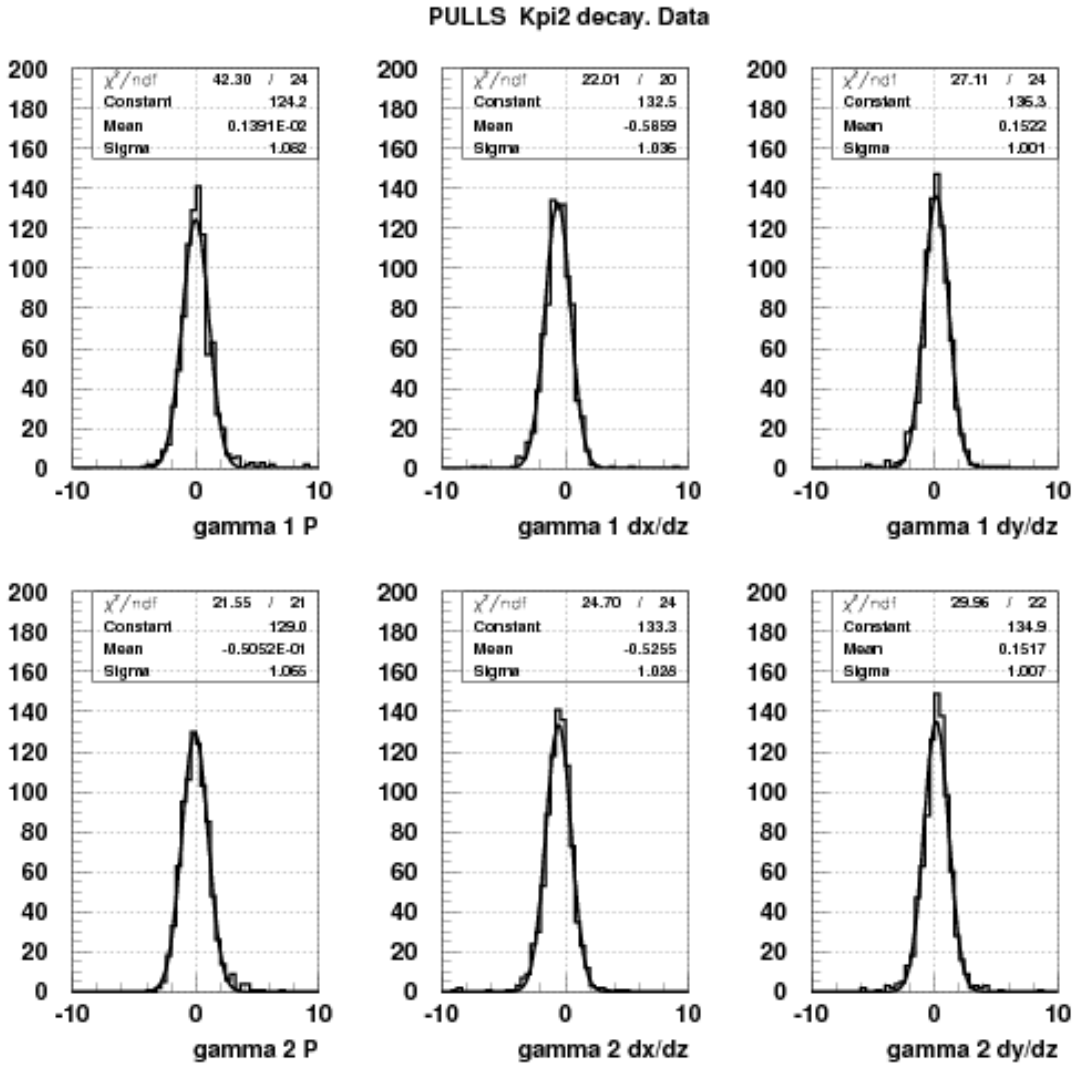

FIG. 10: Data: Pulls for momenta $\mathbf{p}$ (first column) and slopes (dx/dz, dy/dz), for the two gammas (one per row).

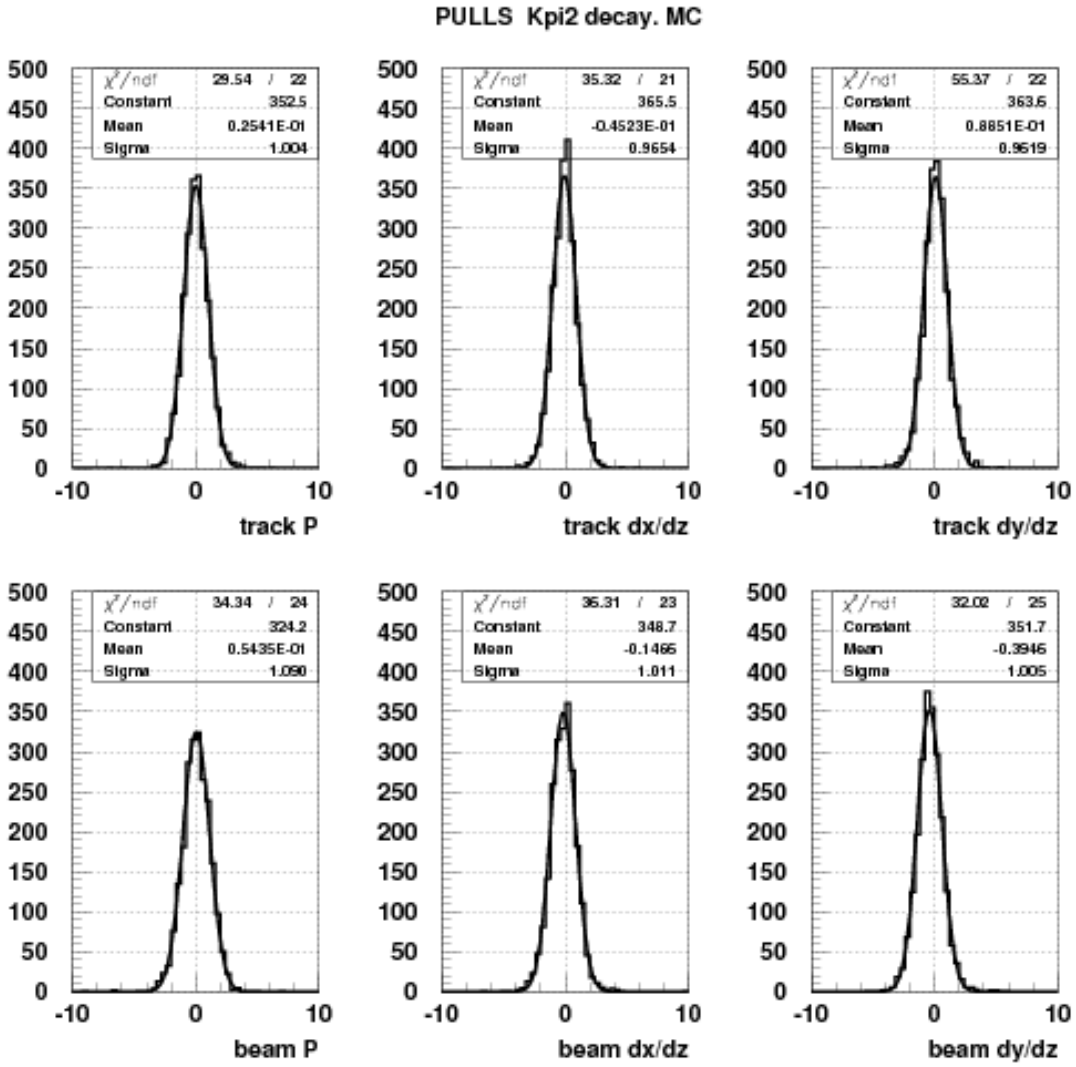

FIG. 11: Monte Carlo: Pulls for momenta **p** (first column) and slopes (dx/dz, dy/dz), for the pion track (top row) and beam (bottom row).

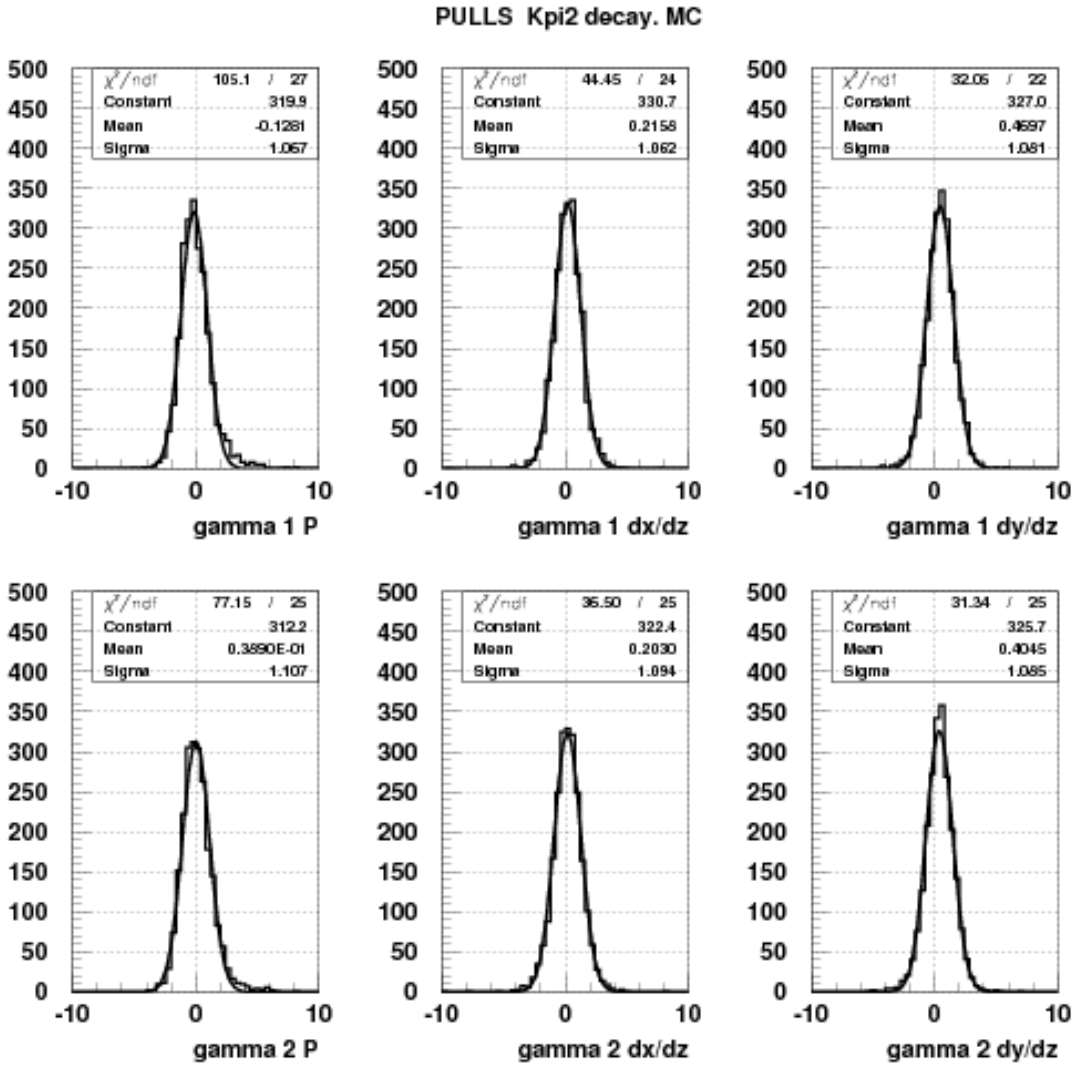

FIG. 12: Monte Carlo: Pulls for momenta **p** (first column) and slopes (dx/dz, dy/dz), for the two γ (one per row).

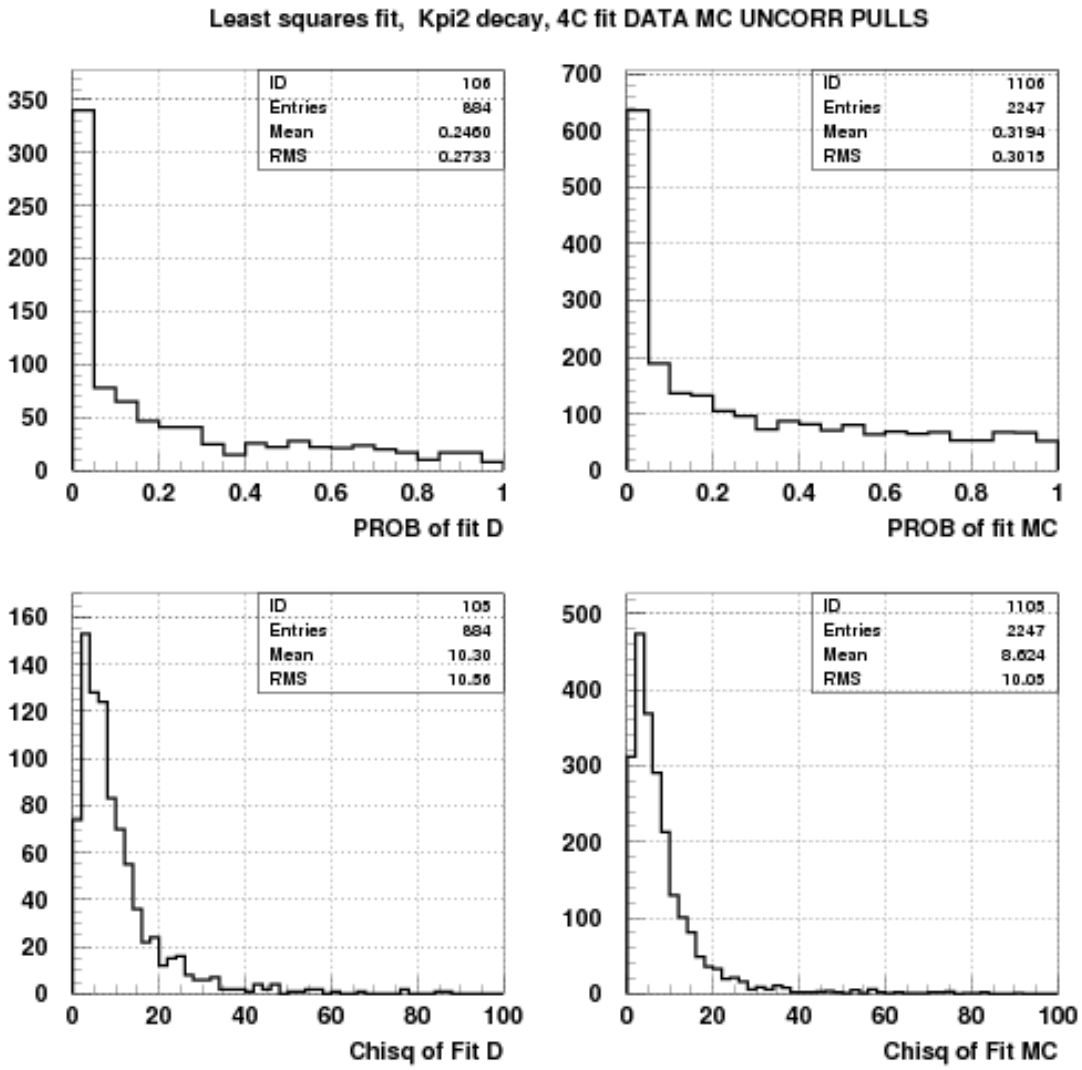

FIG. 13: Probability and χ^2 distributions for data (left column) and MC (right column). Errors uncorrected

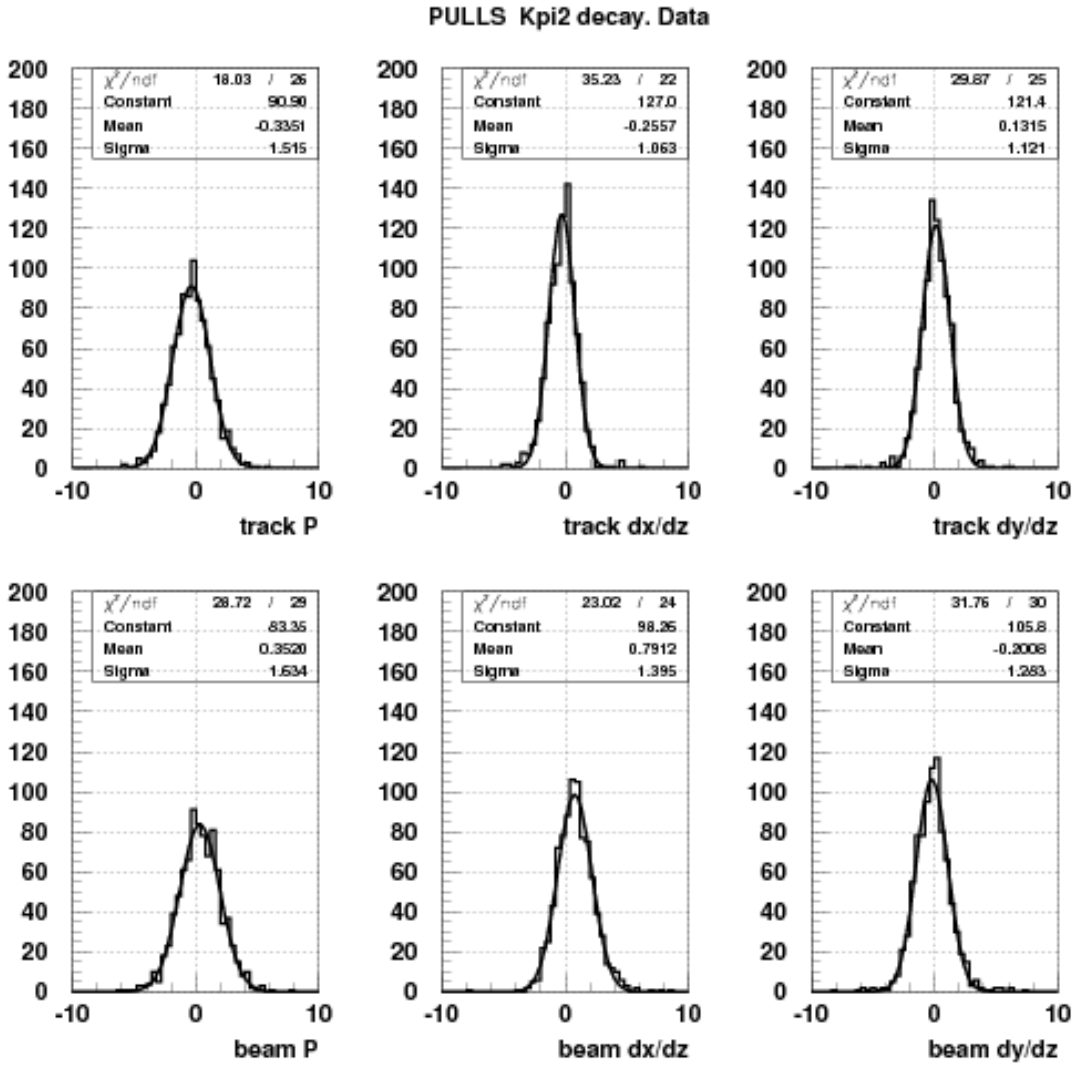

FIG. 14: Data: Pulls for momenta **p** (first column) and slopes (dx/dz, dy/dz), for the pion track (top row) and beam (bottom row). Errors uncorrected.

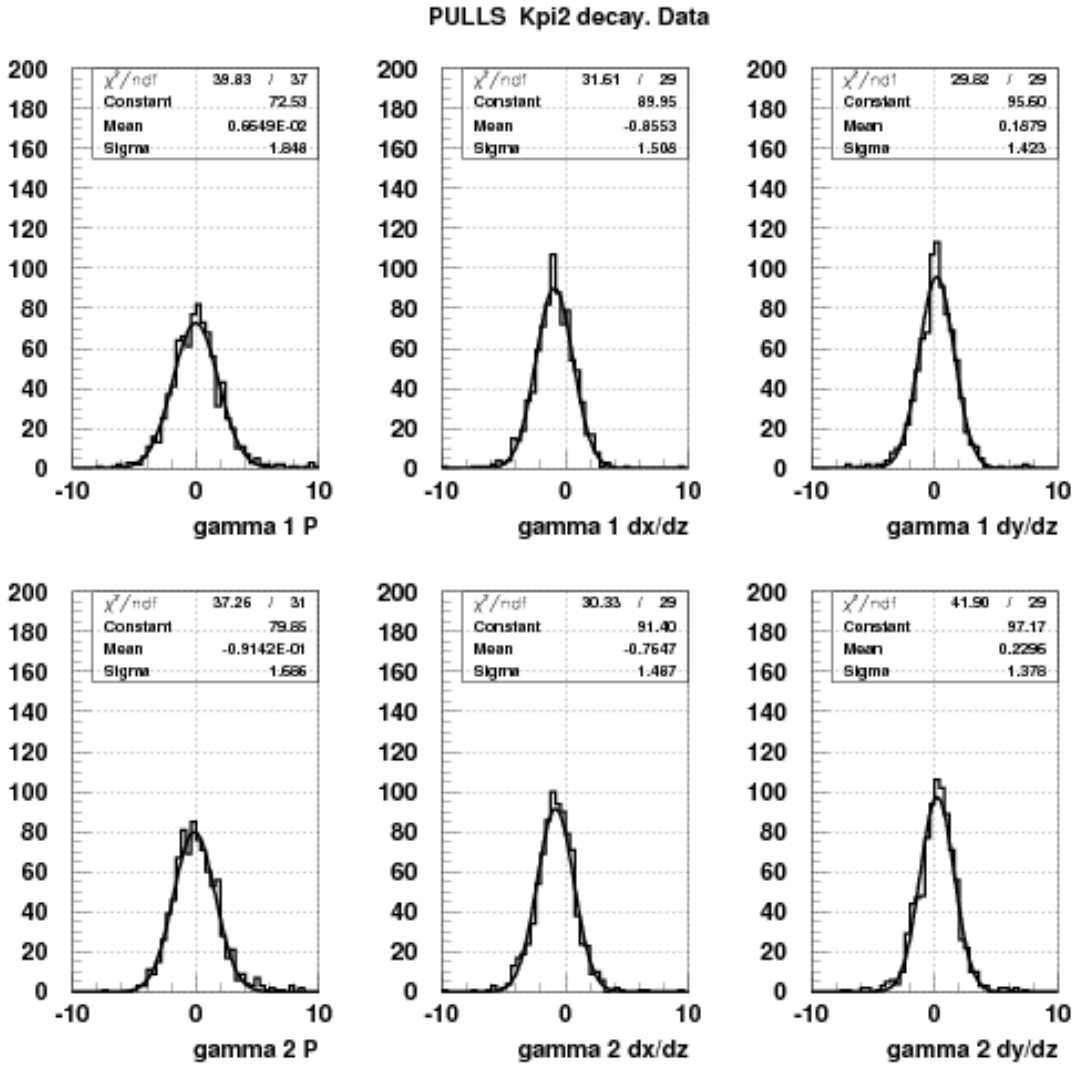

FIG. 15: Data: Pulls for momenta **p** (first column) and slopes (dx/dz, dy/dz), for the two gammas (one per row). Errors uncorrected.

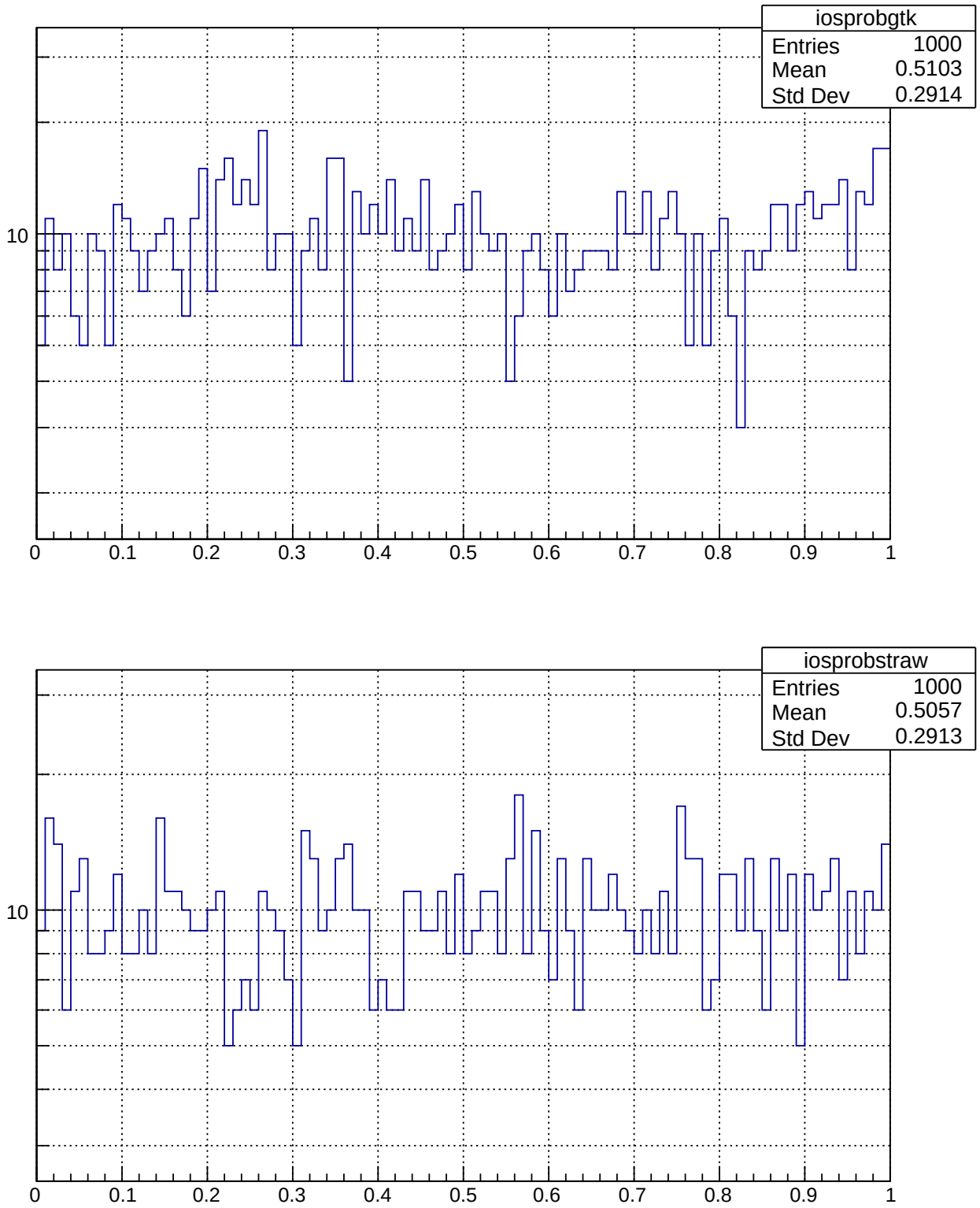

FIG. 16: Probability of the time distribution for the $t_{GKT} - t_{KTAG}$ (top) and $t_{STRAW} - t_{KTAG}$ (bottom).

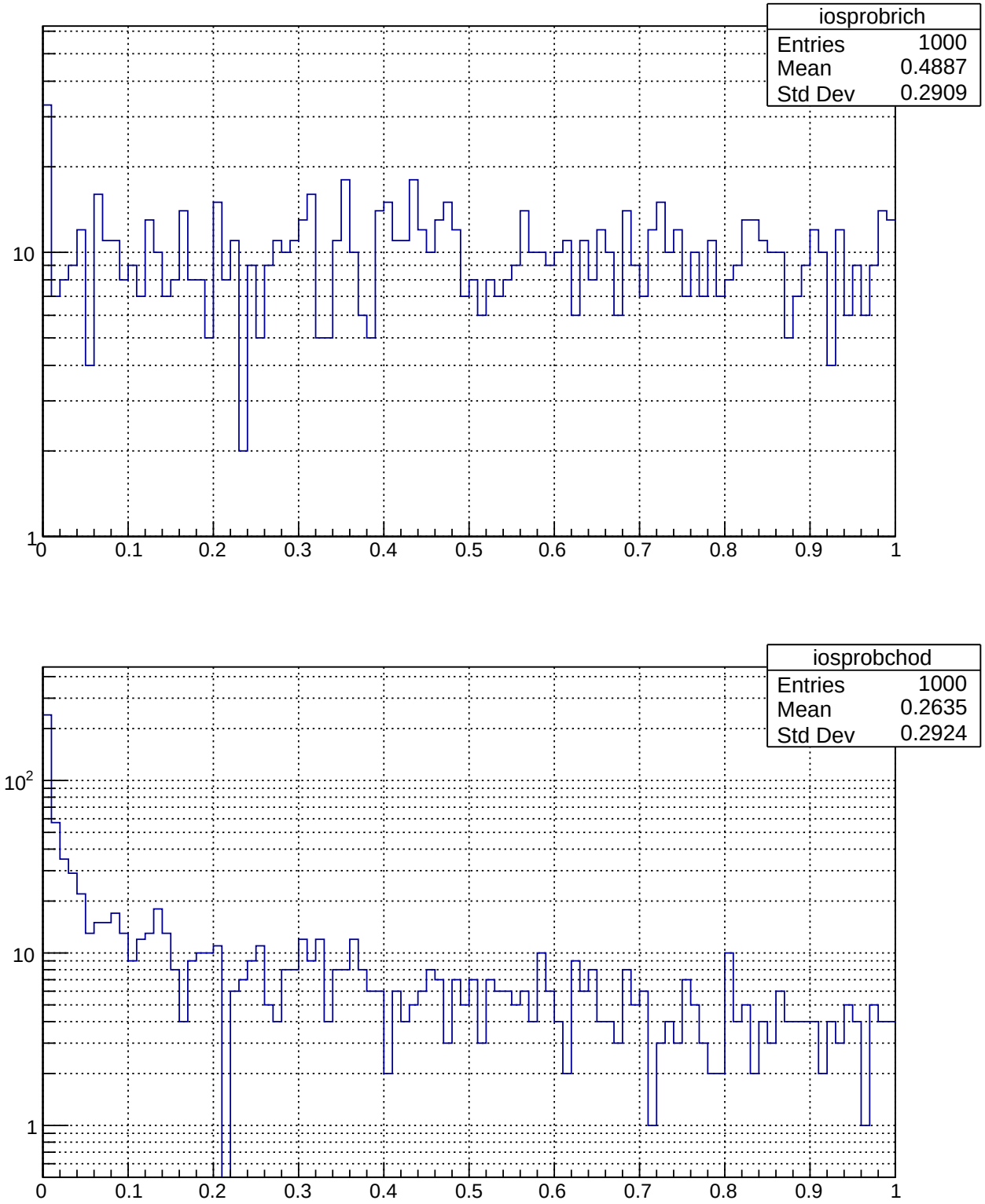

FIG. 17: Probability of the time distribution for $t_{RICH} - t_{KTAG}$ (top), $t_{CHOD} - t_{KTAG}$ (bottom).